World Journal of Radiology

Submit a Manuscript: https://www.f6publishing.com

World J Radiol 2020 October 28; 12(10): 231-246

DOI: 10.4329/wjr.v12.i10.231

ISSN 1949-8470 (online)

ORIGINAL ARTICLE

Basic Study

Cardiac functional magnetic resonance imaging at 7T: Image quality optimization and ultra-high field capabilities

El-Sayed H Ibrahim, V Emre Arpinar, L Tugan Muftuler, Jadranka Stojanovska, Andrew S Nencka, Kevin M Koch

ORCID number: El-Sayed H Ibrahim 0000-0003-4292-4669; V Emre Arpinar 0000-0002-3238-4569; L Tugan Muftuler 0000-0002-6635-5678; Jadranka Stojanovska 0000-0003-2742-6274; Andrew S Nencka 0000-0001-5268-2718; Kevin M Koch 0000-0003-4490-9761.

Author contributions: Ibrahim EH helped with study design, experiments, image and data analysis, results interpretation, and manuscript writing; Arpinar VE helped with experiments, image and data analysis, and manuscript revision; Muftuler LT helped with study design, experiments, and manuscript revision; Stojanovska J helped with results interpretation and manuscript revision; Nencka AS helped with results interpretation and manuscript revision; Koch KM helped with results interpretation and manuscript revision; and all authors read and approved the final manuscript.

Supported by The Daniel M. Soref Charitable Trust, Center for Imaging Research, Medical College of Wisconsin, United States.

Institutional review board statement: This study was conducted with approval from

El-Sayed H Ibrahim, V Emre Arpinar, Andrew S Nencka, Kevin M Koch, Department of Radiology, Medical College of Wisconsin, Milwaukee, WI 53226, United States

L Tugan Muftuler, Department of Neurosurgery, Medical College of Wisconsin, Milwaukee, WI 53226, United States

Jadranka Stojanovska, Department of Radiology, University of Michigan, Ann Arbor, MI 48109, United States

Corresponding author: El-Sayed H Ibrahim, PhD, Associate Professor, Department of Radiology, Medical College of Wisconsin, 8701 Watertown Plank Rd, Milwaukee, WI 53226, United States. eibrahim@mcw.edu

Abstract

BACKGROUND

7T cardiac magnetic resonance imaging (MRI) introduces several advantages, as well as some limitations, compared to lower-field imaging. The capabilities of ultra-high field (UHF) MRI have not been fully exploited in cardiac functional imaging.

AIM

To optimize 7T cardiac MRI functional imaging without the need for conducting B1 shimming or subject-specific tuning, which improves scan efficiency. In this study, we provide results from phantom and *in vivo* scans using a multi-channel transceiver modular coil.

METHODS

We investigated the effects of adding a dielectric pad at different locations next to the imaged region of interest on improving image quality in subjects with different body habitus. We also investigated the effects of adjusting the imaging flip angle in cine and tagging sequences on improving image quality, B1 field homogeneity, signal-to-noise ratio (SNR), blood-myocardium contrast-to-noise ratio (CNR), and tagging persistence throughout the cardiac cycle.

RESULTS

The results showed the capability of achieving improved image quality with high spatial resolution (0.75 mm × 0.75 mm × 2 mm), high temporal resolution (20 ms),

Medical College of Wisconsin Institutional Review Board, and informed consent was obtained from scanned human subjects.

Conflict-of-interest statement: The authors have no conflicts-of-interest to report.

Data sharing statement: The datasets used and/or analyzed during the current study are available from the corresponding author on reasonable request.

ARRIVE guidelines statement: The authors have read the ARRIVE guidelines, and the manuscript was prepared and revised according to the ARRIVE guidelines.

Manuscript source: Unsolicited manuscript

Received: July 17, 2020
Peer-review started: July 17, 2020
First decision: September 21, 2020
Revised: September 27, 2020
Accepted: October 13, 2020
Article in press: October 13, 2020
Published online: October 28, 2020

P-Reviewer: Li M, Nassar G
S-Editor: Huang P
L-Editor: A
P-Editor: Wu YXJ

and increased tagging persistence (for up to 1200 ms cardiac cycle duration) at 7T cardiac MRI after adjusting scan set-up and imaging parameters. Adjusting the imaging flip angle was essential for achieving optimal SNR and myocardium-to-blood CNR. Placing a dielectric pad at the anterior left position of the chest resulted in improved B1 homogeneity compared to other positions, especially in subjects with small chest size.

CONCLUSION
Improved regional and global cardiac functional imaging can be achieved at 7T MRI through simple scan set-up adjustment and imaging parameter optimization, which would allow for more streamlined and efficient UHF cardiac MRI.

Key Words: Magnetic resonance imaging; High-field; Cardiac function; Cine; Tagging; Strain

Core Tip: The capabilities of ultra-high-field magnetic resonance imaging (MRI) have not been fully exploited in cardiac functional imaging. In this study, we provide results from phantom and *in vivo* scans using a multi-channel transceiver modular coil to optimize 7T cardiac MRI functional imaging without the need for conducting B1 shimming or subject-specific system tuning. The results showed that improved regional and global cardiac functional imaging can be achieved at 7T MRI through simple scan set-up adjustment and imaging parameter optimization, which would allow for more streamlined and efficient ultra-high-field cardiac MRI with access to more information and details compared to lower-field imaging.

Citation: Ibrahim EH, Arpinar VE, Muftuler LT, Stojanovska J, Nencka AS, Koch KM. Cardiac functional magnetic resonance imaging at 7T: Image quality optimization and ultra-high field capabilities. *World J Radiol* 2020; 12(10): 231-246
URL: https://www.wjgnet.com/1949-8470/full/v12/i10/231.htm
DOI: https://dx.doi.org/10.4329/wjr.v12.i10.231

INTRODUCTION

Cardiac magnetic resonance imaging (MRI) is the gold standard for assessment of cardiac function due to its high resolution and tissue contrast. Cardiac MRI functional imaging can provide information not only about global heart function, *e.g.*, ejection fraction (EF), but also about regional tissue contractility, *e.g.*, myocardial strain using MRI tagging[1], where the latter has shown to reveal early manifestation of subclinical cardiac dysfunction that typically precedes EF reduction[2-6].

Cardiac function assessment using MRI has been established in clinical practice on 1.5T and 3T scanners, where it showed the capability for identification of different cardiovascular diseases, including coronary artery disease, cardiomyopathies, and different valvular, vascular, and congenital heart diseases. Nevertheless, the capabilities of ultra-high field (UHF) MRI have not been fully exploited for cardiac functional imaging, which are expected to improve image quality and provide more information for better understanding of heart mechanics in both normal and pathophysiological conditions; thus, opening the door for new cardiac MRI applications[7-16].

With 7T MRI scanners from different vendors receiving clearance for clinical applications, it might be expected that 7T MRI will soon be adopted in clinical practice[7,8,17,18]. UHF MRI introduces several advantages, as well as some limitations, compared to lower-field imaging. As signal-to-noise ratio (SNR) is proportional to magnetic field strength, 7T MRI provides more than double SNR compared to 3T imaging[19,20]. The enhanced SNR can be traded for improved image quality, higher spatial or temporal resolution, or shorter scan time. Furthermore, due to prolonged T1 relaxation times at 7T, improved tissue contrast can be achieved compared to lower magnetic fields[17]. The advantages of UHF imaging could lead to improved image

quality, illustration of anatomical details, and shorter scan time, which are of particular importance in cardiac functional imaging.

Despite its advantages, high-field imaging at 7T is challenging due to a number of technical issues[9,11,21,22]. First, the applied radiofrequency (RF) field at such high frequency results in short wavelength (approximately 12 cm) and increased dielectric effect that can induce destructive and constructive wave interferences and results in distorted B1 field and non-uniform effective flip angle distribution with observed shading and signal drop-off effects[23,24]. Another challenge of UHF imaging is RF penetration to the posterior wall of the heart, where coils with dipole arrays provide superior penetration depth[25]. Imaging at UHF also results in increased B0 inhomogeneity[26,27] and specific absorption ratio (SAR) and noisy electrocardiogram (ECG) signal[22,28], although these effects are not prohibiting factors of conducting cardiac MRI at 7T. Besides technical challenges, UHF imaging could result in some undesirable effects on imaged subjects, where dizziness, nausea, metallic taste, light flashes, and peripheral nerve stimulations have been reported[7,10,29]. Nevertheless, there has been no significant clinical complications experienced at 7T MRI.

A promising technique for addressing B1 inhomogeneity in UHF imaging relies on parallel transmission methods[30,31] using multiple transmit RF channels[19,23,32]. Recent efforts have been made for developing multi-channel transceiver surface coil arrays tailored for UHF imaging[9,21,23,24,32-35]. The capability of independently modulating each coil element's magnitude and phase allows for producing more uniform B1 field with less signal inhomogeneity across the imaged region while maintaining SAR within allowable limits. Furthermore, the modular design of such multi-channel coils allows for close fitting with the body, more patient's comfort, and suitability for clinical applications[23,24]. The capabilities of combining multi-channel parallel imaging and simultaneous multi-slice acquisition for improving imaging efficiency have been recently investigated[36].

In this study, we provide preliminary results from phantom and *in vivo* scans using a multi-channel transceiver modular coil to optimize 7T cardiac MRI functional imaging without the need for conducting B1 shimming or subject-specific tuning, which improve scan efficiency. We investigate the effects of adding a dielectric pad at different locations next to the imaged region of interest on improving image quality in subjects with different body habitus. We also investigate the effects of adjusting the imaging flip angle in cine and tagging sequences on improving image quality, B1 field homogeneity, SNR, blood-myocardium contrast-to-noise ratio (CNR), and tagging persistence throughout the cardiac cycle.

MATERIALS AND METHODS

Experiments set-up

This study was conducted with approval from our Institutional Review Board and informed consent was obtained from scanned human subjects. A static phantom and twelve healthy subjects were scanned on a GE MR950 7T whole-body scanner (GE Healthcare, Milwaukee, United States) equipped with peak gradient amplitude and maximum slew rate of 50 mT/m and 200 T/m/s, respectively and using a 32-channel transceiver coil (MRI Tools, GmbH, Berlin, Germany). The modular coil array consists of 8 independent blocks: Four blocks located posteriorly in a planar fashion and four blocks located anteriorly in a bent fashion, which provide close fit to the chest with stable loading condition[9,37]. Each coil block contains 4 transceiver elements (2 × 2 array), whose phase settings were optimized based on simulations for a multi-oblique plane mimicking a standard cardiac view[37]. The coil elements are arranged in an interleaved fashion so that they are shifted from each other by a half-element size[9].

B1 mapping

We conducted phantom and *in vivo* scans to generate an estimate of the B1 transmission frequency field in the imaged slice using the actual flip-angle imaging B1 mapping method[38,39]. A spoiled gradient echo cine sequence was used for repeated image acquisitions with nominal flip angles ranging from 1° to 120°, and forward simulation was conducted on the resulting images. To overcome the inherent motion problem in cardiac imaging, lowpass filtering was conducted to mitigate the motion problem and achieve better B1 estimates.

SAR calculations

The MRI system first looks at the predicted global SAR, which is vendor-provided SAR tables specific to the coil used and its imaging mode (cardiac mode in this case). The 32 channels of the coil are grouped in blocks of four elements each with fixed inter-element phases for the transmission mode. The MRI system then calculates local SAR over a 10 g mass sample for the worst-case scenario using different virtual body models, as previously explained[40,41]. Upon comparing local and global SAR calculations, the more conservative one is taken into consideration and used for all scans.

Effect of imaging flip angle on image quality

Both cine and tagging images were acquired in the volunteers in standard cardiac short-axis and long-axis views, which are typically used for measuring cardiac functional parameters, *e.g.*, EF. The coil placement and prescription flip angle were adjusted to improve image quality. Specifically, the effect of modifying the prescribed flip angle from 10° to 90° on myocardium SNR and myocardium-to-blood CNR was studied. Myocardial SNR was measured as the ratio between mean signal intensity in the myocardium divided by standard deviation (SD) of background noise. CNR was measured as the difference between mean signal intensities in blood and myocardium divided by SD of background noise.

The imaging parameters for cine imaging were as follows: Fast spoiled gradient echo sequence, repetition time (TR) = 8 ms, echo time (TE) = 4 ms, flip angle = 60°, matrix = 256 × 256, field-of-view (FOV) = 380 mm × 380 mm, slice thickness = 8 mm, acquisition bandwidth = 244 Hz/pixel, number of averages = 1, and number of cardiac phases = 25. The imaging parameters for the tagging sequence were as follows: Fast gradient echo sequence, TR = 4.9 ms, TE = 2 ms, flip angle = 15°, matrix = 256 × 256, FOV = 380 mm × 380 mm, slice thickness = 8 mm, acquisition bandwidth = 488 Hz/pixel, number of averages = 1, and number of cardiac phases = 25.

Myocardial tagging persistence at 7T

The elevated T_1 value of normal myocardium at 7T (approximately 1900 ms at 7T compared to approximately 1150 ms and approximately 850 ms at 3T and 1.5T, respectively[9,42]) results in slower magnetization recovery towards equilibrium, and thus helps reduce taglines fading during later phases of the cardiac cycle. We conducted Bloch simulation to investigate the effect of elevated T_1 value at 7T on improving tagging persistence compared to that at 1.5T. Furthermore, we used the sinusoidal modulation technique[43] to analyze the tagged images and measure myocardial strain in a subject with low heart rate of 50 beats per minute (bpm; cardiac cycle length = 1200 ms).

Effect of using a dielectric pad on image quality

We investigated the effect of adding a dielectric pad (30 cm × 40 cm flexible pad from GE Healthcare, part number E8823JA) close to the imaged slice on improving B1 homogeneity. As moving the dielectric pad around the thorax area affects the presence and location of signal nulling regions, we studied the effect of changing the pad's position in eight volunteers with different body habitus and chest size, which were divided into two groups. Group 1 consisted of four volunteers (2 males, 2 females) with small body habitus: Healthy-weight body mass index (BMI < 25 kg/m^2) = 22.5 ± 2.5 kg/m^2, chest expansion in the anterior-posterior and left-right directions = 24.8 ± 3.2 cm and 31.3 ± 2.2 cm, respectively. Group 2 consisted of four volunteers (2 males, 2 females) with larger body habitus: Overweight BMI (> 25 kg/m^2) = 26.4 ± 1.1 kg/m^2, chest expansion in the anterior-posterior and left-right directions = 28.8 ± 1.7 cm and 31.5 ± 2.4 cm, respectively.

RESULTS

With proper scan set-up and imaging parameter settings, all subjects were successfully scanned with good image quality. The ECG signal was reliable in all scans and image acquisition was correctly triggered at the R-wave, despite elevated T wave and noisier ECG signal compared to the case at lower magnetic fields.

B1 mapping

Figures 1 and 2 show results from phantom and volunteer scans, respectively, to

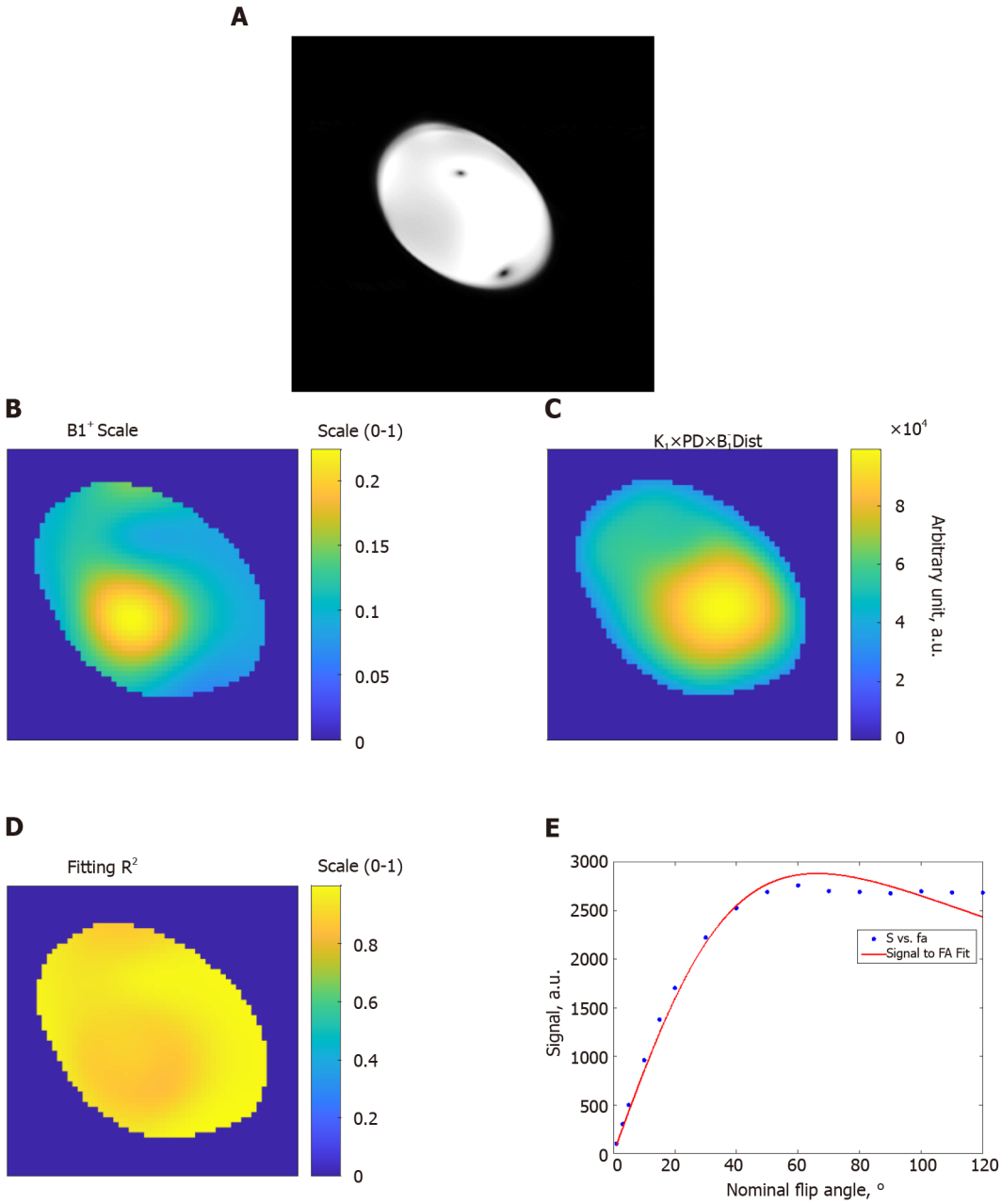

Figure 1 Estimation of the B1 transmission field in a homogeneous phantom. A: Gradient-echo magnitude image of the phantom; B: B1 scale factor map (range, 0 to 1) of the phantom; C: Proton density distribution map (arbitrary units; a.u.); D: R^2 fitting map (range, 0 to 1) shows excellent simulation fittings; E: Example of signal intensity measurements (arbitrary units; a.u.) at different flip angles in degrees (dots) and the fitting curve inside the phantom. The results show altered B1 field across the imaged slice. FA: Flip angle.

estimate the B1 field. The figures show signal intensity variation across the acquired slices, where the signal intensity profile changes with the prescribed flip angle. The estimated B1 map and proton density distribution reflect the observed signal intensity in the imaged slices, and the resulting R^2 fitting maps show excellent data fitting.

SAR calculations

Figure 3 shows maximum intensity projections of 10 g-averaged SAR normalized to 1W forward power at the coil plug using male and female virtual body models for a cardiac imaging[40]. Differences between male and female body habitus were taken into consideration for the virtual model simulation. For example, a breast mass of 490 g was used for female body simulation to account for the effects of the mammary glands on resulting calculations and their effect on image characteristics, *e.g.*, signal nulling or contrast variation[40]. During volunteer scans, SAR is limited based on the chosen excitation mode[41], where worst-case scenario among different body models is taken into consideration and used for all cases. Figure 3 also shows local and global SAR

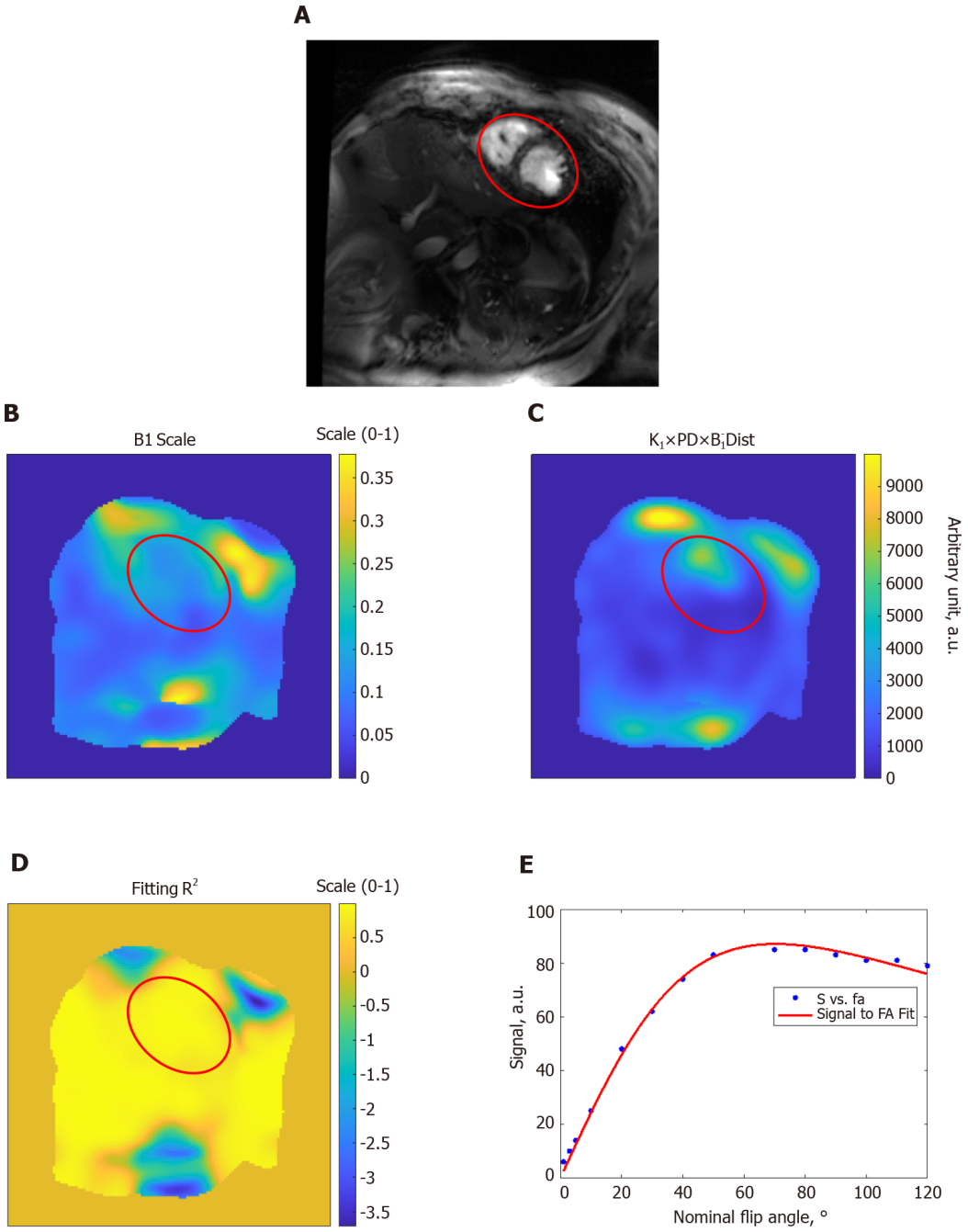

Figure 2 Estimation of the B1 transmission field in a volunteer scan. A: Gradient-echo short-axis image; B: B1 scale factor map (range, 0 to 1); C: Proton density distribution map (arbitrary units; a.u.); D: R^2 fitting map (range, 0 to 1) shows excellent simulation fittings; E: Example of signal intensity measurements (arbitrary units; a.u.) at different flip angles in degrees (dots) and the fitting curve inside the heart region (red circle). The results show altered B1 field across the imaged slice. FA: Flip angle.

values as reported by the Dicom tags for *in vivo* cine imaging with different flip angles, where local SAR is the limiting factor for SAR calculations.

Experiments set-up and imaging flip angle effects on image quality

We found that moving the coil up towards the chin of the imaged subject (average of 5 cm offset shift of the coil center from heart center) resulted in improved signal intensity, especially at the basal and lateral regions of the heart, compared to when the coil was centered around the heart. The prescribed imaging flip angle played a key role in determining SNR and CNR (Figure 4). Due to the difference between nominal and actual flip angles at 7T imaging, as shown in Figures 1 and 2, the prescribed flip angle for gradient echo cine imaging at 7T needed to be much higher than that used at 1.5T and 3T fields (approximately 10°-20°). Based on results from this study, a prescribed flip angle of approximately 60° resulted in sufficient RF penetration and

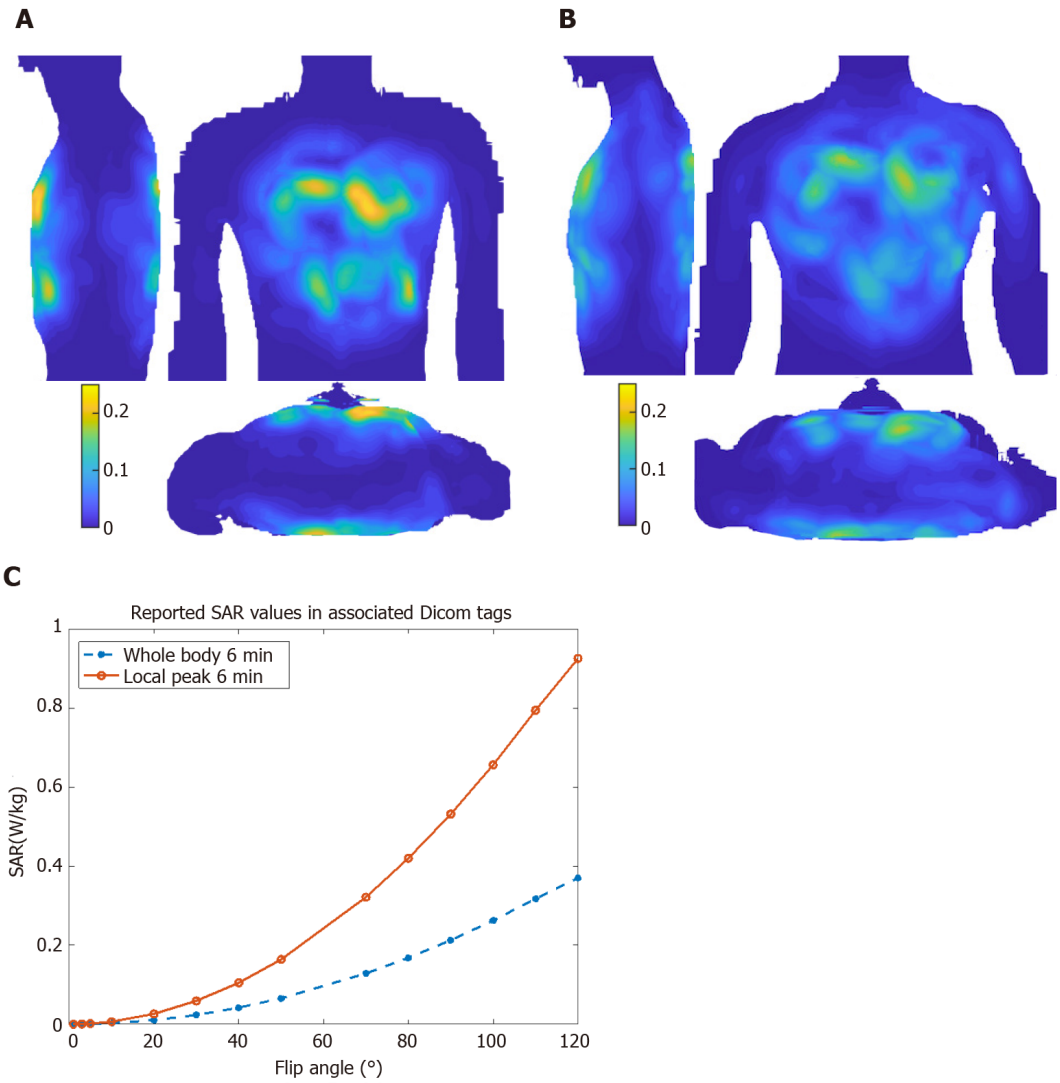

Figure 3 Specific absorption ratio calculations. Maximum intensity projections of 10 g-averaged specific absorption ratio (SAR) normalized to 1W forward power at the coil plug using male 'Duke' (A) and female 'Ella' (B) virtual body modes; C: Reported SAR values for different flip angle from the cine scan Dicom tags in the subject in Figure 2. SAR: Specific absorption ratio.

improved image quality. In the example shown in Figure 4, a 60° flip angle resulted in optimal SNR/CNR of 181/116, which is much higher than those reported at lower magnetic fields, for example SNR/CNR of 79/43 at 1.5T[44].

Improved cine and tagging imaging at 7T

With high SNR at 7T, high spatial resolution can be achieved compared to that available at lower field strength. Figure 5 shows a high-resolution cine image with voxel size of 0.75 mm × 0.75 mm × 2 mm and the same slice acquired with conventional resolution of 1.5 mm × 1.5 mm × 8 mm that is typically used in clinical practice on 1.5T and 3T scanners. The high-resolution image shows fine anatomical details of the trabecula, papillary muscles, and right ventricle that appear blurry at conventional resolution. Otherwise, high SNR can be traded for improved temporal resolution, where we were able to achieve cine imaging with 20 ms temporal resolution (50 frames for a heart rate of 60 bpm) at conventional spatial resolution reported above.

Figures 6 and 7 show the effect of elevated myocardial T_1 value and large field strength at 7T on improving tagging persistence. Figure 6 shows the results of Bloch simulation of the tagging pattern evolution during a 1200 ms cardiac cycle (50 bpm heart rate) for both 7T and 1.5T field strengths. The slow magnetization recovery at 7T resulted in maintaining more than half (53%) of the original tagging contrast (measured as the peak-to-peak difference in signal intensity of the tagging pattern) by the end of the 1200 ms cardiac cycle at 7T, compared to only 24% of the original tagging contrast at 1.5T. When taking the field strength effect into consideration, then

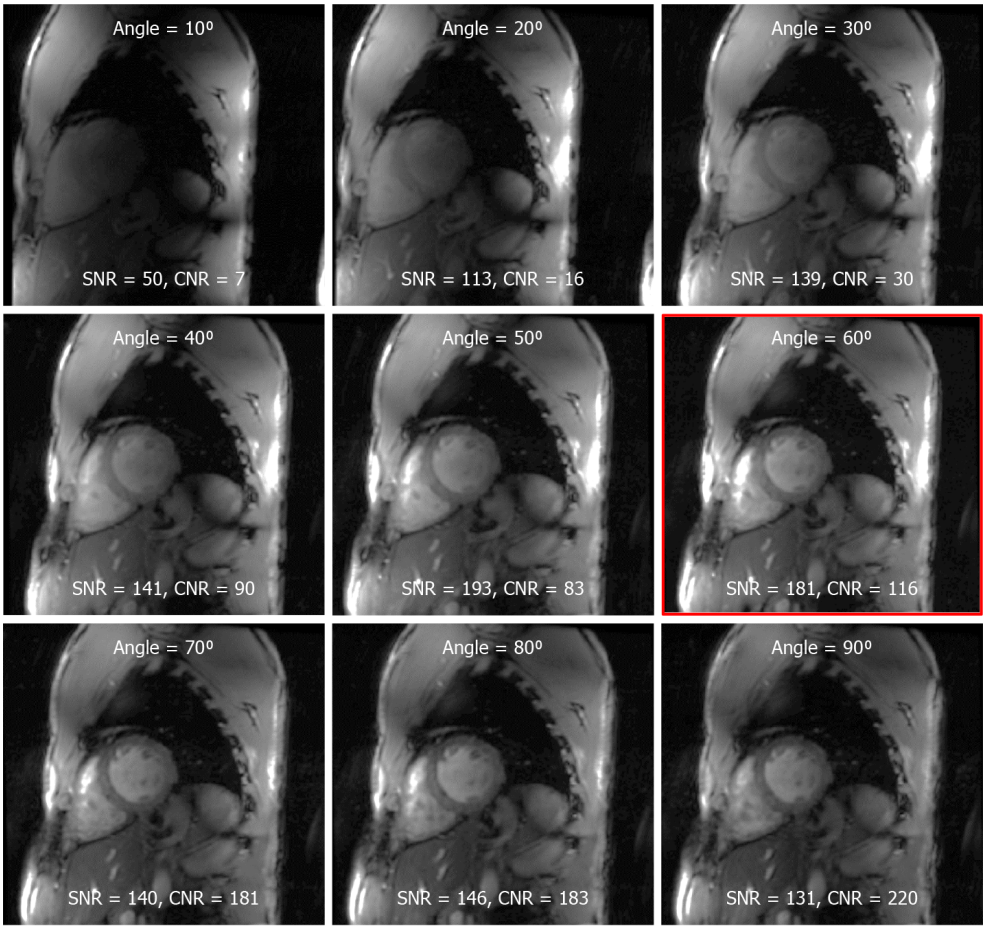

Figure 4 The effect of the prescribed flip angle on myocardium signal-to-noise ratio and blood-to-myocardium contrast-to-noise ratio. Optimal signal-to-noise ratio (SNR) was achieved at prescribed flip angle of approximately 60° (red framed image). Although higher flip angles resulted in better blood-to-myocardium contrast-to-noise ratio, this came at the cost of reduced SNR. SNR: Signal-to-noise ratio; CNR: Contrast-to-noise ratio.

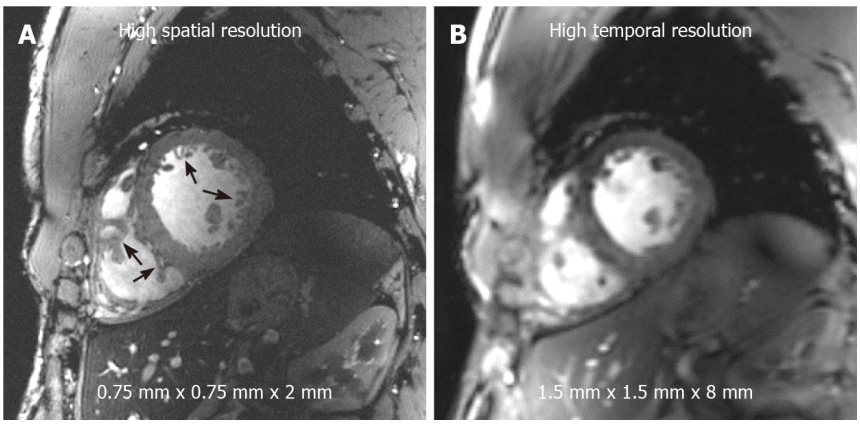

Figure 5 Improved image resolution achieved at 7T cardiac magnetic resonance imaging. High signal-to-noise ratio (SNR) at 7T allows for achieving high spatial resolution with 16-fold reduction in voxel size (A) compared to standard clinical resolution in (B). Small voxel size illustrates anatomical details, such as the trabeculations and right ventricle details (arrows), that are not clearly visible at standard clinical resolution. Alternatively, high SNR can be traded for high temporal resolution (approximately 20 ms) imaging at conventional spatial resolution as in (B).

there is a reduction of 90% in tagging contrast when switching from 7T to 1.5T by the end the 1200 ms cardiac cycle. Therefore, it is typically difficult to measure myocardial strain at later diastolic cardiac phases for low-field imaging due to fading of the tagging pattern, which is not the case at 7T, as shown by the *in vivo* results in Figure 7 of a subject with heart rate of 50 bpm, where the tagging pattern was visible throughout the whole cardiac cycle and allowed for measuring strain throughout end-diastole. It should be noted that optimal prescribed flip angle for tagging MRI was 15°,

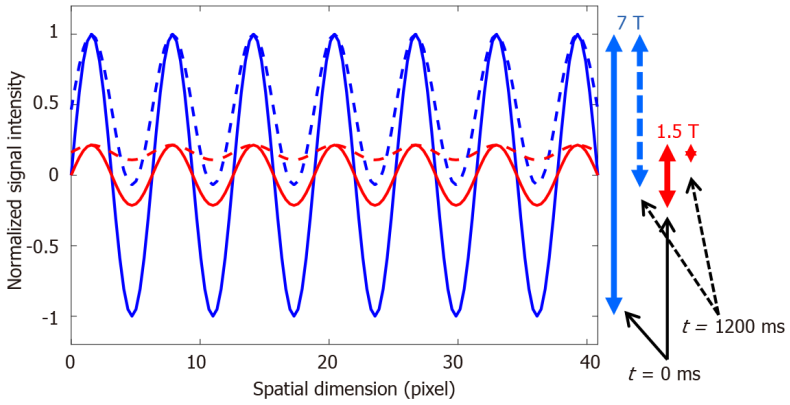

Figure 6 Improved tagging persistence at 7T cardiovascular magnetic resonance. Numerical simulation of the effect of magnetic field strength on the tagging pattern persistence. The tagging patterns (blue, 7T; red, 1.5T) have maximum contrast (peak-to-peak difference) immediately after tagging creation at the beginning of the cardiac cycle (time = 0 ms), as represented by the solid lines. Note the difference in tagging contrast (vertical solid arrows on the right) corresponding to the difference in field strength. With time, longitudinal magnetization experiences exponential relaxation trying to reach equilibrium with different T_1 values of the myocardium depending on the magnetic field strength (T_1 = 850 ms and 1900 ms are used for 1.5T and 7T, respectively). By the end of a 1200 ms cardiac cycle (assuming heart rate of 50 bpm), the tagging patterns have experienced fading (dotted lines), such that there is a significant difference in tagging contrast between 7T and 1.5T, as represented by the vertical dotted arrows on the right, which results in diminished visibility of the tagging pattern by the end of the cardiac cycle at the low field strength.

as larger flip angles resulted in faster fading of the taglines. On the other hand, lower flip angles resulted in poor tissue contrast.

Improving B1 homogeneity using a dielectric pad

The effect of the dielectric pad's position on improving B1 uniformity was impacted by the imaged subject's body habitus (Figures 8 and 9). For volunteers with small-to-medium weight (BMI < 25 kg/m^2), placing the pad at the anterior left position of the chest (the volunteers were scanned in the supine position) resulted in improved B1 uniformity compared to other anterior and posterior positions, as shown in Figure 8. This behavior was consistent in all scanned volunteer with small-to-medium body habitus. On the other hand, in volunteers with larger body habitus (BMI > 25 kg/m^2), B1 uniformity was acceptable even without using the dielectric pad, and it was similar to the case when the pad was positioned in the anterior left position of the chest, as shown in Figure 9. Moving the pad to other positions resulted in less B1 uniformity and appearance of regions with signal nulling. This behavior was consistent in all scanned volunteers with large body habitus.

DISCUSSION

While the majority of UHF studies have focused on brain and orthopedic applications, recent improvements in multi-channel coil development opened the door for cardiac imaging to benefit from UHF MRI capabilities[9-11]. The results from this study show that high-quality global (cine) and regional (tagging) cardiac functional imaging can be obtained at 7T by simple optimization of the scan set-up and imaging parameters, especially to mitigate B1-related signal inhomogeneity effects.

Adjusting the prescription flip angle and adding a dielectric pad next to the imaged region-of-interest helped improve B1 homogeneity and reduce signal nulling artifacts. The actual flip angle across the heart can vary by as much as 50% from the nominal flip angle, even at 3T[45], which is imperative in certain applications that use 180° RF pulses as in fast spin-echo imaging and inversion-recovery-based T_1 mapping[42]. Nevertheless, these constraints can be loosened in gradient-echo-based cardiac functional imaging by increasing the prescription flip angle to ensure sufficient RF penetration to the whole heart and generation of images with good SNR and tissue contrast.

It should be noted that shallow flip angle (15°) was used in acquisition of the tagged images, compared to 60° in the case of cine images, in order to maintain the tagging pattern throughout the whole cardiac cycle. Although larger flip angle results in better myocardium-to-blood contrast, it results in more tipping of the magnetization vector into the transverse plane, and therefore the magnetization pattern fades quickly due to

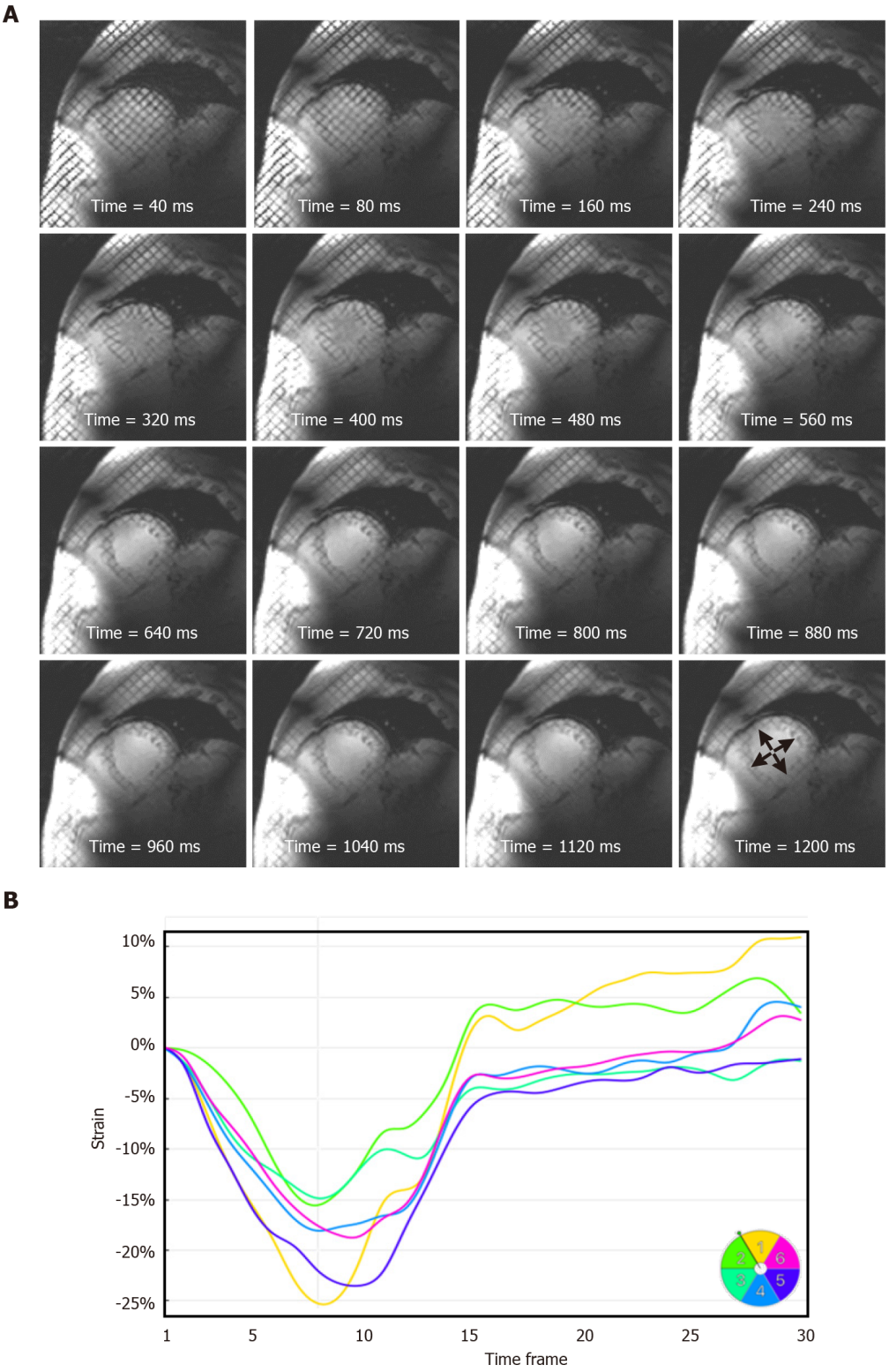

Figure 7 Strain analysis throughout the whole cardiac cycle at 7T cardiovascular magnetic resonance. A: A series of tagged images acquired at different timepoints of a mid-ventricular short-axis slice throughout a 1200 ms cardiac cycle, showing tagging persistence until the last timeframe (arrows), which allows for measuring strain throughout end-diastole, which is not feasible at low magnetic field strength where the tagging pattern fades before the end of the cardiac cycle; B: Circumferential strain curves showing strain evolution throughout the whole cardiac cycle in different left-ventricular myocardial segments of the slice in (A). Segments are numbered according to American Heart Association 17-segment model.

short T2 relaxation time of the myocardium (approximately 50 ms). On the contrary, using a shallow flip angle allows for maintaining the tagging pattern for a long time due to slow longitudinal magnetization recovery with long myocardial T1 relaxation time (approximately 1900 ms). It should be noted that the shallow flip angle does not affect the tagging-to-myocardium contrast as the tag lines appear dark due to

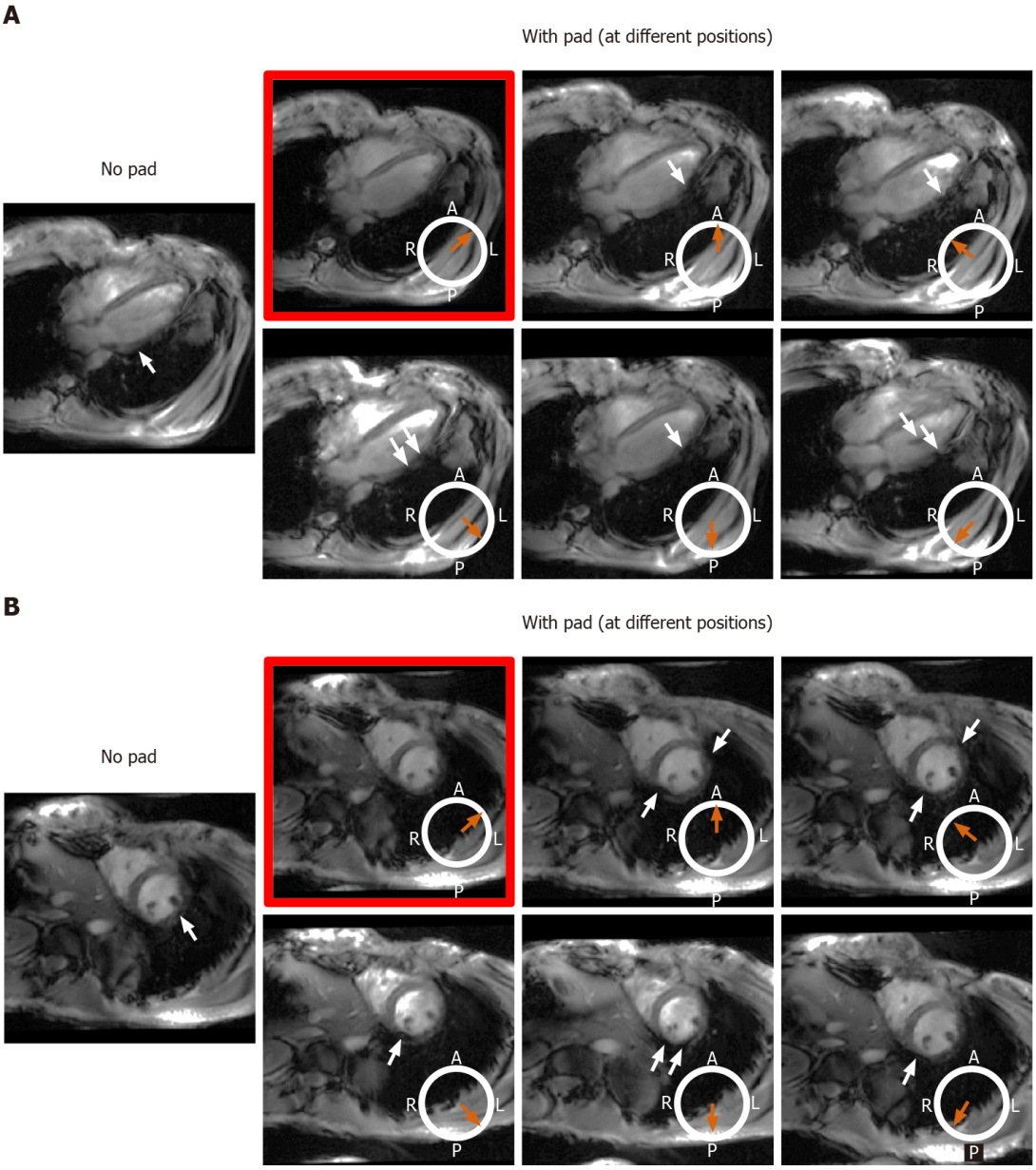

Figure 8 The effect of changing location of the dielectric pad on B1 field homogeneity in volunteers with small body habitus. The place of the pad is indicated by the orange arrow with respect to an axial cross-section of the subject's chest region (white circle, where subject was scanned in the supine position; A: Anterior, P: Posterior, L: Left, R: Right). Results from an underweight volunteer [body mass index = 19 kg/m^2, chest expansions = 20 cm (AP) and 30 cm (LR)], as shown on long-axis (A) and short-axis (B) slices. Placing the pad at the anterior left position of the chest (image with red frame) resulted in improved B1 uniformity compared to other anterior and posterior positions, which showed regions of signal nulling (white arrows). This behavior was consistent in all scanned subjects with small body habitus.

magnetization saturation during the tagging preparation step. Furthermore, because the tagging pattern is maintained in the myocardium and destroyed in the blood pool, due to blood motion, there is still good contrast between myocardium and blood in the tagged images.

Adding a dielectric pad next to the imaged region of interest and properly adjusting its location based on body habitus resulted in generating a more homogeneous B1 field around the heart, rendering patient-specific tuning and matching of individual coil elements unnecessary in this study, which helps streamline UHF cardiac imaging. Specifically, the results showed that: (1) Adding a dielectric pad had more effect on improving B1 homogeneity in subjects with small body habitus compared to subjects with large body habitus; and (2) Placing the dielectric pad in the anterior left position of the chest resulted in improved B1 homogeneity compared to other anterior and posterior positions. These results can be understood in light of the dielectric pad's effect on changing B1 distribution in its vicinity, which is affected by the coil loading as a result of specific body habitus. Generally, the dielectric pad helps improve

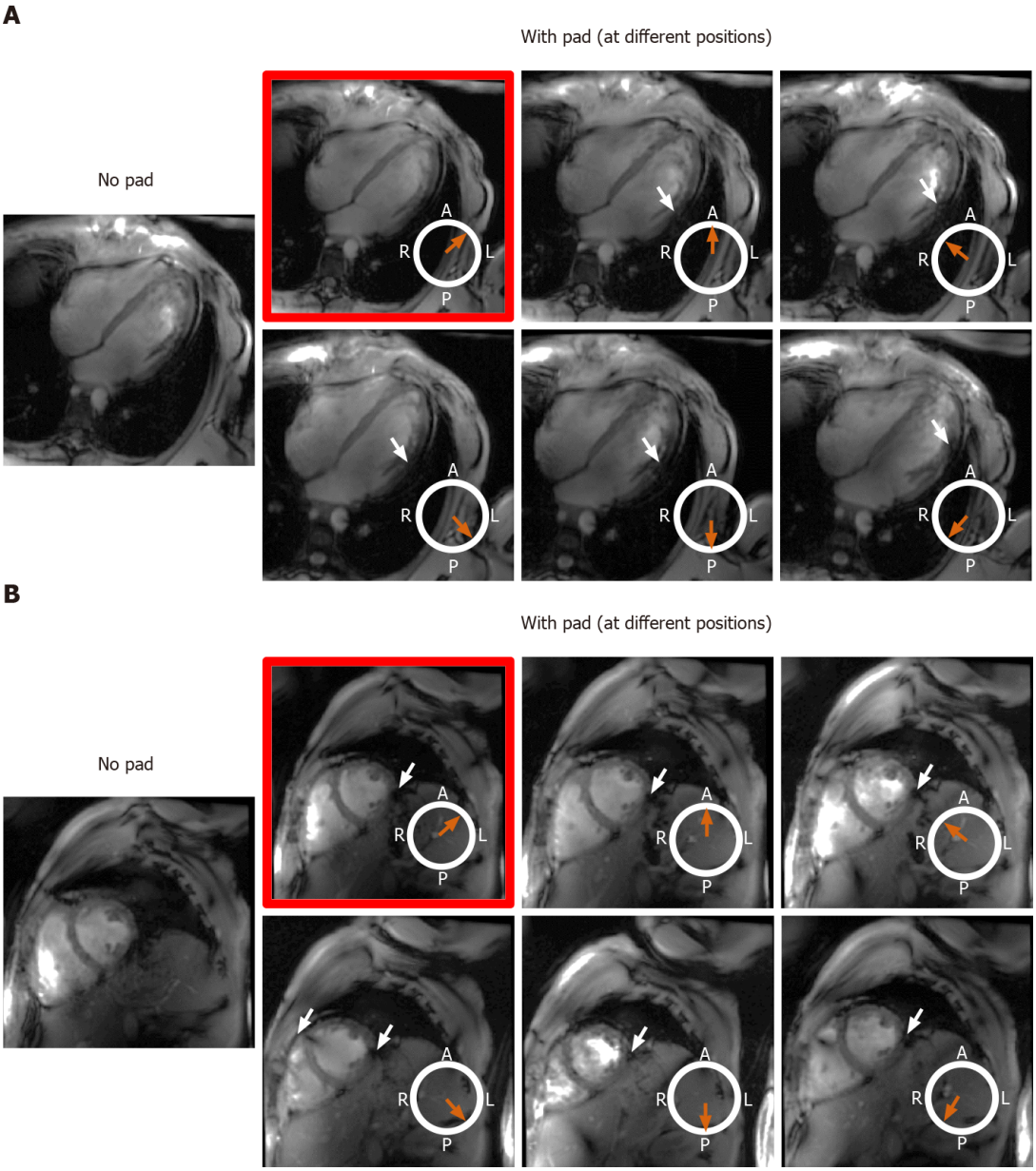

Figure 9 The effect of changing location of the dielectric pad on B1 field homogeneity in volunteers with large body habitus. The place of the pad is indicated by the orange arrow with respect to an axial cross-section of the subject's chest region (white circle, where subject was scanned in the supine position; A: Anterior, P: Posterior, L: Left, R: Right). Results from an overweight volunteer [body mass index = 26.1 kg/m^2, chest expansions = 27 cm (AP) and 30 cm (LR)], as shown on long-axis (A) and short-axis (B) slices. B1 uniformity was acceptable without using the pad (image on the left), which was similar to the case when the pad was positioned in the anterior left position of the chest (image with red frame). Changing the pad position resulted in slightly worse B1 uniformity, as shown by regions of signal nulling (white arrows). This behavior was consistent in all scanned subjects with large body habitus.

impedance matching for B1 field propagation[46]. Furthermore, the secondary local RF field in the pad enhances the original B1 field. The more effect noticed in subjects with small body habitus could be understood, in part, by the more pronounced standing wave effect in subjects with small chest area compared to those with larger chest area. The more effect of the dielectric pad when placed in the anterior left position could be understood because the pad is closest to the heart in this position, and thus has more effect on changing the B1 field around the heart.

Intrinsic characteristics of UHF imaging, *e.g.*, prolonged myocardium T_1 values, can be a key advantage for cardiac MRI tagging. As shown in this study, the prolonged myocardium T_1 value resulted in improved tagging persistence throughout the whole cardiac cycle even at slow heart rates, which allowed for analyzing the myocardial contractility pattern until end-diastole, an appreciated feature considering the rapid taglines fading during late cardiac phases in conventional low-field imaging.

In this study, we showed the capability of 7T cardiac MRI for generating high-resolution cardiac cine images with voxel size that is 16 times smaller than that in

clinical standards. Such high spatial resolution allows for visualizing detailed anatomical features without sacrificing SNR as one would expect in lower field MRI. This feature is appreciated in applications when high-fidelity anatomical details need to be imaged, *e.g.*, in pediatric imaging, congenital heart diseases, diffusion tensor imaging of myofiber tractography, right ventricle imaging[44], and for patient triaging in certain cardiomyopathies[47]. Alternatively, the extra SNR in 7T MRI can be traded for high temporal resolution in applications where accurate measurements require high temporal resolution, *e.g.*, flow imaging[13] and time-resolved cine imaging of patients with fast heart rate.

The transceiver modular coil used in this study allowed for obtaining high-quality *in vivo* images with high resolution and adequate myocardium-to-blood contrast. Future coil developments with increased number of RF transceiver elements would allow for even more improvement in scan performance and parallel imaging capability. Other advancements in developing shorter, actively shielded, and wider bore 7T magnets would allow for more adoption of UHF cardiac MRI in clinical practice.

One limitation of the current study is the limited number of studied subjects, which does not allow for conducting a thorough statistical analysis. Nevertheless, our goal in this study was to provide a proof-of-concept of improved quality 7T cardiac MRI cine and tagging imaging and illustrate achieved advantages compared to low-field imaging capabilities. To the best of our knowledge, this is the first study to focus on this important application, especially the effect of adding a dielectric pad on improving signal homogeneity and the capability of improving tagging imaging and strain analysis at 7T. Nevertheless, more studies on a larger cohort are warranted to confirm the results from this study and to investigate more details, *e.g.*, the effect of the dielectric pad size or material on the results.

CONCLUSION

In conclusions, improved cardiac functional imaging can be achieved at 7T through simple scan set-up and imaging parameter adjustments, which would allow for more streamlined and efficient UHF cardiac imaging with more adoption in clinical practice and access to more information and details compared to lower-field imaging.

ARTICLE HIGHLIGHTS

Research background

Magnetic resonance imaging (MRI) is the gold standard for assessment of cardiac function, which can provide information not only about global heart function, but also about regional tissue contractility patterns. With 7T MRI scanners from different vendors receiving clearance for clinical applications, it might be expected that 7T cardiac MRI will soon be adopted in clinical practice to get benefit from ultra-high field (UHF) capabilities.

Research motivation

The capabilities of UHF cardiac MRI have not been fully exploited in cardiac functional imaging, which are expected to improve image quality and provide more information compared to imaging capabilities at current clinical magnetic field strengths.

Research objectives

To optimize 7T cardiac MRI functional imaging without the need for conducting B1 shimming or subject-specific system tuning, which improves scan efficiency.

Research methods

We conducted both phantom and *in vivo* scans using a multi-channel transceiver modular coil. We investigated the effects of adding a dielectric pad at different locations next to the imaged region of interest on improving image quality in subjects with different body habitus. We also investigated the effects of adjusting the imaging flip angle in cine and tagging sequences on improving image quality, B1 field homogeneity, signal-to-noise ratio (SNR), blood-myocardium contrast-to-noise ratio

(CNR), and tagging persistence throughout the cardiac cycle.

Research results

The results showed the capability of achieving improved image quality with high spatial resolution, high temporal resolution, and increased tagging persistence at 7T cardiac MRI after adjusting scan set-up and imaging parameters. Adjusting the imaging flip angle was essential for achieving optimal SNR and myocardium-to-blood CNR. Placing a dielectric pad at the anterior left position of the chest resulted in improved B1 homogeneity compared to other positions, especially in subjects with small chest size.

Research conclusions

Improved regional and global cardiac functional imaging can be achieved at 7T MRI through simple scan set-up adjustment and imaging parameter optimization, which allows for access to more information and details compared to lower-field MRI.

Research perspectives

The developed optimized MRI exam would allow for more streamlined and efficient UHF cardiac functional imaging. Future studies should investigate the clinical usefulness of the developed technique by implementing it on large number of patients with different cardiovascular diseases.

REFERENCES

1 **Manning WJ**, Pennell DJ. Cardiovascular Magnetic Resonance: A Companion to Braunwald's Heart Disease. 3rd ed. Elsevier, 2018

2 **Ibrahim EH**. Heart Mechanics: Magnetic Resonance Imaging—The Complete Guide. 1st ed. CRC Press, 2017

3 **Kongbundansuk S**, Hundley WG. Noninvasive imaging of cardiovascular injury related to the treatment of cancer. *JACC Cardiovasc Imaging* 2014; **7**: 824-838 [PMID: 25124015 DOI: 10.1016/j.jcmg.2014.06.007]

4 **Choi EY**, Rosen BD, Fernandes VR, Yan RT, Yoneyama K, Donekal S, Opdahl A, Almeida AL, Wu CO, Gomes AS, Bluemke DA, Lima JA. Prognostic value of myocardial circumferential strain for incident heart failure and cardiovascular events in asymptomatic individuals: the Multi-Ethnic Study of Atherosclerosis. *Eur Heart J* 2013; **34**: 2354-2361 [PMID: 23644181 DOI: 10.1093/eurheartj/eht133]

5 **Wong DT**, Leong DP, Weightman MJ, Richardson JD, Dundon BK, Psaltis PJ, Leung MC, Meredith IT, Worthley MI, Worthley SG. Magnetic resonance-derived circumferential strain provides a superior and incremental assessment of improvement in contractile function in patients early after ST-segment elevation myocardial infarction. *Eur Radiol* 2014; **24**: 1219-1228 [PMID: 24723232 DOI: 10.1007/s00330-014-3137-6]

6 **Toro-Salazar OH**, Gillan E, O'Loughlin MT, Burke GS, Ferranti J, Stainsby J, Liang B, Mazur W, Raman SV, Hor KN. Occult cardiotoxicity in childhood cancer survivors exposed to anthracycline therapy. *Circ Cardiovasc Imaging* 2013; **6**: 873-880 [PMID: 24097420 DOI: 10.1161/CIRCIMAGING.113.000798]

7 **Niendorf T**, Paul K, Oezerdem C, Graessl A, Klix S, Huelnhagen T, Hezel F, Rieger J, Waiczies H, Frahm J, Nagel AM, Oberacker E, Winter L. W(h)ither human cardiac and body magnetic resonance at ultrahigh fields? *NMR Biomed* 2016; **29**: 1173-1197 [PMID: 25706103 DOI: 10.1002/nbm.3268]

8 **Snyder CJ**, DelaBarre L, Metzger GJ, van de Moortele PF, Akgun C, Ugurbil K, Vaughan JT. Initial results of cardiac imaging at 7 Tesla. *Magn Reson Med* 2009; **61**: 517-524 [PMID: 19097233 DOI: 10.1002/mrm.21895]

9 **Niendorf T**, Graessl A, Thalhammer C, Dieringer MA, Kraus O, Santoro D, Fuchs K, Hezel F, Waiczies S, Ittermann B, Winter L. Progress and promises of human cardiac magnetic resonance at ultrahigh fields: a physics perspective. *J Magn Reson* 2013; **229**: 208-222 [PMID: 23290625 DOI: 10.1016/j.jmr.2012.11.015]

10 **Niendorf T**, Sodickson DK, Krombach GA, Schulz-Menger J. Toward cardiovascular MRI at 7 T: clinical needs, technical solutions and research promises. *Eur Radiol* 2010; **20**: 2806-2816 [PMID: 20676653 DOI: 10.1007/s00330-010-1902-8]

11 **von Knobelsdorff-Brenkenhoff F**, Frauenrath T, Prothmann M, Dieringer MA, Hezel F, Renz W, Kretschel K, Niendorf T, Schulz-Menger J. Cardiac chamber quantification using magnetic resonance imaging at 7 Tesla--a pilot study. *Eur Radiol* 2010; **20**: 2844-2852 [PMID: 20640427 DOI: 10.1007/s00330-010-1888-2]

12 **Brandts A**, Westenberg JJ, Versluis MJ, Kroft LJ, Smith NB, Webb AG, de Roos A. Quantitative assessment of left ventricular function in humans at 7 T. *Magn Reson Med* 2010; **64**: 1471-1477 [PMID: 20593368 DOI: 10.1002/mrm.22529]

13 **Hess AT**, Bissell MM, Ntusi NA, Lewis AJ, Tunnicliffe EM, Greiser A, Stalder AF, Francis JM, Myerson SG, Neubauer S, Robson MD. Aortic 4D flow: quantification of signal-to-noise ratio as a function of field strength and contrast enhancement for 1.5T, 3T, and 7T. *Magn Reson Med* 2015; **73**: 1864-1871 [PMID: 24934930 DOI: 10.1002/mrm.25317]

14 **Huelnhagen T**, Hezel F, Serradas Duarte T, Pohlmann A, Oezerdem C, Flemming B, Seeliger E, Prothmann M, Schulz-Menger J, Niendorf T. Myocardial effective transverse relaxation time T2* Correlates with left ventricular wall thickness: A 7.0 T MRI study. *Magn Reson Med* 2017; **77**: 2381-2389 [PMID: 27342430 DOI: 10.1002/mrm.26312]

15 **Tao Y**, Hess AT, Keith GA, Rodgers CT, Liu A, Francis JM, Neubauer S, Robson MD. Optimized saturation pulse train for human first-pass myocardial perfusion imaging at 7T. *Magn Reson Med* 2015; **73**: 1450-1456 [PMID: 24753130 DOI: 10.1002/mrm.25262]

16 **Harteveld AA**, van der Kolk AG, Zwanenburg JJ, Luijten PR, Hendrikse J. 7-T MRI in Cerebrovascular Diseases: Challenges to Overcome and Initial Results. *Top Magn Reson Imaging* 2016; **25**: 89-100 [PMID: 27049246 DOI: 10.1097/RMR.0000000000000080]

17 **Stäb D**, Al Najjar A, O'Brien K, Strugnell W, Richer J, Rieger J, Niendorf T, Barth M. Cardiac Magnetic Resonance Imaging at 7 Tesla. *J Vis Exp* 2019; : [PMID: 30663648 DOI: 10.3791/55853]

18 **Hoff MN**, McKinney A 4th, Shellock FG, Rassner U, Gilk T, Watson RE Jr, Greenberg TD, Froelich J, Kanal E. Safety Considerations of 7-T MRI in Clinical Practice. *Radiology* 2019; **292**: 509-518 [PMID: 31310177 DOI: 10.1148/radiol.2019182742]

19 **Pohmann R**, Speck O, Scheffler K. Signal-to-noise ratio and MR tissue parameters in human brain imaging at 3, 7, and 9.4 tesla using current receive coil arrays. *Magn Reson Med* 2016; **75**: 801-809 [PMID: 25820458 DOI: 10.1002/mrm.25677]

20 **Erturk MA**, Li X, Van de Moortele PF, Ugurbil K, Metzger GJ. Evolution of UHF Body Imaging in the Human Torso at 7T: Technology, Applications, and Future Directions. *Top Magn Reson Imaging* 2019; **28**: 101-124 [PMID: 31188271 DOI: 10.1097/RMR.0000000000000202]

21 **Steensma BR**, Voogt IJ, Leiner T, Luijten PR, Habets J, Klomp DWJ, van den Berg CAT, Raaijmakers AJE. An 8-channel Tx/Rx dipole array combined with 16 Rx loops for high-resolution functional cardiac imaging at 7 T. *MAGMA* 2018; **31**: 7-18 [PMID: 29177772 DOI: 10.1007/s10334-017-0665-5]

22 **van Elderen SG**, Versluis MJ, Webb AG, Westenberg JJ, Doornbos J, Smith NB, de Roos A, Stuber M. Initial results on *in vivo* human coronary MR angiography at 7 T. *Magn Reson Med* 2009; **62**: 1379-1384 [PMID: 19859918 DOI: 10.1002/mrm.22168]

23 **Gräßl A**, Winter L, Thalhammer C, Renz W, Kellman P, Martin C, von Knobelsdorff-Brenkenhoff F, Tkachenko V, Schulz-Menger J, Niendorf T. Design, evaluation and application of an eight channel transmit/receive coil array for cardiac MRI at 7.0 T. *Eur J Radiol* 2013; **82**: 752-759 [PMID: 21920683 DOI: 10.1016/j.ejrad.2011.08.002]

24 **Thalhammer C**, Renz W, Winter L, Hezel F, Rieger J, Pfeiffer H, Graessl A, Seifert F, Hoffmann W, von Knobelsdorff-Brenkenhoff F, Tkachenko V, Schulz-Menger J, Kellman P, Niendorf T. Two-dimensional sixteen channel transmit/receive coil array for cardiac MRI at 7.0 T: design, evaluation, and application. *J Magn Reson Imaging* 2012; **36**: 847-857 [PMID: 22706727 DOI: 10.1002/jmri.23724]

25 **Ertürk MA**, Raaijmakers AJ, Adriany G, Uğurbil K, Metzger GJ. A 16-channel combined loop-dipole transceiver array for 7 Tesla body MRI. *Magn Reson Med* 2017; **77**: 884-894 [PMID: 26887533 DOI: 10.1002/mrm.26153]

26 **Spincemaille P**, Anderson J, Wu G, Yang B, Fung M, Li K, Li S, Kovanlikaya I, Gupta A, Kelley D, Benhamo N, Wang Y. Quantitative Susceptibility Mapping: MRI at 7T *versus* 3T. *J Neuroimaging* 2020; **30**: 65-75 [PMID: 31625646 DOI: 10.1111/jon.12669]

27 **Stockmann JP**, Wald LL. *In vivo* B_0 field shimming methods for MRI at 7T. *Neuroimage* 2018; **168**: 71-87 [PMID: 28602943 DOI: 10.1016/j.neuroimage.2017.06.013]

28 **Frauenrath T**, Hezel F, Heinrichs U, Kozerke S, Utting JF, Kob M, Butenweg C, Boesiger P, Niendorf T. Feasibility of cardiac gating free of interference with electro-magnetic fields at 1.5 Tesla, 3.0 Tesla and 7.0 Tesla using an MR-stethoscope. *Invest Radiol* 2009; **44**: 539-547 [PMID: 19652614 DOI: 10.1097/RLI.0b013e3181b4c15e]

29 **Klix S**, Els A, Paul K, Graessl A, Oezerdem C, Weinberger O, Winter L, Thalhammer C, Huelnhagen T, Rieger J, Mehling H, Schulz-Menger J, Niendorf T. On the subjective acceptance during cardiovascular magnetic resonance imaging at 7.0 Tesla. *PLoS One* 2015; **10**: e0117095 [PMID: 25621491 DOI: 10.1371/journal.pone.0117095]

30 **Orzada S**, Solbach K, Gratz M, Brunheim S, Fiedler TM, Johst S, Bitz AK, Shooshtary S, Abuelhaija A, Voelker MN, Rietsch SHG, Kraff O, Maderwald S, Flöser M, Oehmigen M, Quick HH, Ladd ME. A 32-channel parallel transmit system add-on for 7T MRI. *PLoS One* 2019; **14**: e0222452 [PMID: 31513637 DOI: 10.1371/journal.pone.0222452]

31 **Rietsch SHG**, Orzada S, Bitz AK, Gratz M, Ladd ME, Quick HH. Parallel transmit capability of various RF transmit elements and arrays at 7T MRI. *Magn Reson Med* 2018; **79**: 1116-1126 [PMID: 28394080 DOI: 10.1002/mrm.26704]

32 **Schmitter S**, Wu X, Uğurbil K, Van de Moortele PF. Design of parallel transmission radiofrequency pulses robust against respiration in cardiac MRI at 7 Tesla. *Magn Reson Med* 2015; **74**: 1291-1305 [PMID: 25411131 DOI: 10.1002/mrm.25512]

33 **Winter L**, Kellman P, Renz W, Gräßl A, Hezel F, Thalhammer C, von Knobelsdorff-Brenkenhoff F, Tkachenko V, Schulz-Menger J, Niendorf T. Comparison of three multichannel transmit/receive radiofrequency coil configurations for anatomic and functional cardiac MRI at 7.0T: implications for clinical imaging. *Eur Radiol* 2012; **22**: 2211-2220 [PMID: 22653280 DOI: 10.1007/s00330-012-2487-1]

34 **Ruytenberg T**, Webb A, Zivkovic I. Shielded-coaxial-cable coils as receive and transceive array elements for 7T human MRI. *Magn Reson Med* 2020; **83**: 1135-1146 [PMID: 31483530 DOI: 10.1002/mrm.27964]

35 **Yan X**, Zhang X, Gore JC, Grissom WA. Improved traveling-wave efficiency in 7T human MRI using passive local loop and dipole arrays. *Magn Reson Imaging* 2017; **39**: 103-109 [PMID: 28189821 DOI: 10.1016/j.mri.2017.02.003]

36 **Schmitter S**, Moeller S, Wu X, Auerbach EJ, Metzger GJ, Van de Moortele PF, Uğurbil K. Simultaneous multislice imaging in dynamic cardiac MRI at 7T using parallel transmission. *Magn Reson Med* 2017; **77**: 1010-1020 [PMID: 26949107 DOI: 10.1002/mrm.26180]

37 **Graessl A**, Renz W, Hezel F, Dieringer MA, Winter L, Oezerdem C, Rieger J, Kellman P, Santoro D, Lindel TD, Frauenrath T, Pfeiffer H, Niendorf T. Modular 32-channel transceiver coil array for cardiac MRI at 7.0T. *Magn Reson Med* 2014; **72**: 276-290 [PMID: 23904404 DOI: 10.1002/mrm.24903]

38 **Yarnykh VL**. Actual flip-angle imaging in the pulsed steady state: a method for rapid three-dimensional

mapping of the transmitted radiofrequency field. *Magn Reson Med* 2007; **57**: 192-200 [PMID: 17191242 DOI: 10.1002/mrm.21120]

39 **Schmitter S**, DelaBarre L, Wu X, Greiser A, Wang D, Auerbach EJ, Vaughan JT, Uğurbil K, Van de Moortele PF. Cardiac imaging at 7 Tesla: Single- and two-spoke radiofrequency pulse design with 16-channel parallel excitation. *Magn Reson Med* 2013; **70**: 1210-1219 [PMID: 24038314 DOI: 10.1002/mrm.24935]

40 **Christ A**, Kainz W, Hahn EG, Honegger K, Zefferer M, Neufeld E, Rascher W, Janka R, Bautz W, Chen J, Kiefer B, Schmitt P, Hollenbach HP, Shen J, Oberle M, Szczerba D, Kam A, Guag JW, Kuster N. The Virtual Family--development of surface-based anatomical models of two adults and two children for dosimetric simulations. *Phys Med Biol* 2010; **55**: N23-N38 [PMID: 20019402 DOI: 10.1088/0031-9155/55/2/N01]

41 **Eichfelder G**, Gebhardt M. Local specific absorption rate control for parallel transmission by virtual observation points. *Magn Reson Med* 2011; **66**: 1468-1476 [PMID: 21604294 DOI: 10.1002/mrm.22927]

42 **Rodgers CT**, Piechnik SK, Delabarre LJ, Van de Moortele PF, Snyder CJ, Neubauer S, Robson MD, Vaughan JT. Inversion recovery at 7 T in the human myocardium: measurement of T(1), inversion efficiency and B(1) (+). *Magn Reson Med* 2013; **70**: 1038-1046 [PMID: 23197329 DOI: 10.1002/mrm.24548]

43 **Arts T**, Prinzen FW, Delhaas T, Milles JR, Rossi AC, Clarysse P. Mapping displacement and deformation of the heart with local sine-wave modeling. *IEEE Trans Med Imaging* 2010; **29**: 1114-1123 [PMID: 20335094 DOI: 10.1109/TMI.2009.2037955]

44 **von Knobelsdorff-Brenkenhoff F**, Tkachenko V, Winter L, Rieger J, Thalhammer C, Hezel F, Graessl A, Dieringer MA, Niendorf T, Schulz-Menger J. Assessment of the right ventricle with cardiovascular magnetic resonance at 7 Tesla. *J Cardiovasc Magn Reson* 2013; **15**: 23 [PMID: 23497030 DOI: 10.1186/1532-429X-15-23]

45 **Suttie JJ**, Delabarre L, Pitcher A, van de Moortele PF, Dass S, Snyder CJ, Francis JM, Metzger GJ, Weale P, Ugurbil K, Neubauer S, Robson M, Vaughan T. 7 Tesla (T) human cardiovascular magnetic resonance imaging using FLASH and SSFP to assess cardiac function: validation against 1.5 T and 3 T. *NMR Biomed* 2012; **25**: 27-34 [PMID: 21774009 DOI: 10.1002/nbm.1708]

46 **Yang QX**, Mao W, Wang J, Smith MB, Lei H, Zhang X, Ugurbil K, Chen W. Manipulation of image intensity distribution at 7.0 T: passive RF shimming and focusing with dielectric materials. *J Magn Reson Imaging* 2006; **24**: 197-202 [PMID: 16755543 DOI: 10.1002/jmri.20603]

47 **Prothmann M**, von Knobelsdorff-Brenkenhoff F, Töpper A, Dieringer MA, Shahid E, Graessl A, Rieger J, Lysiak D, Thalhammer C, Huelnhagen T, Kellman P, Niendorf T, Schulz-Menger J. High Spatial Resolution Cardiovascular Magnetic Resonance at 7.0 Tesla in Patients with Hypertrophic Cardiomyopathy - First Experiences: Lesson Learned from 7.0 Tesla. *PLoS One* 2016; **11**: e0148066 [PMID: 26863618 DOI: 10.1371/journal.pone.0148066]

Published by **Baishideng Publishing Group Inc**
7041 Koll Center Parkway, Suite 160, Pleasanton, CA 94566, USA
Telephone: +1-925-3991568
E-mail: bpgoffice@wjgnet.com
Help Desk: https://www.f6publishing.com/helpdesk
https://www.wjgnet.com